HHS Public Access

Author manuscript

Mol Neurobiol. Author manuscript; available in PMC 2023 April 01.

Published in final edited form as:

Mol Neurobiol. 2022 April ; 59(4): 2389–2406. doi:10.1007/s12035-021-02624-2.

Cortical dysplasia in rats provokes neurovascular alterations, GLUT1 dysfunction and metabolic disturbances that are sustained post-seizure induction

Chaitali Ghosh[1,2], **Rosemary Myers**[1], **Christina O'Connor**[3], **Sherice Williams**[1], **Xuefeng Liu**[4], **Mohammed Hossain**[1], **Michael Nemeth**[3], **Imad M. Najm**[3]

[1]Cerebrovascular Research, Department of Biomedical Engineering, Lerner Research Institute, Cleveland Clinic, Cleveland, Ohio, USA

[2]Department of Biomedical Engineering and Molecular Medicine, Cleveland Clinic Lerner College of Medicine of Case Western Reserve University, Cleveland, Ohio, USA

[3]Charles Shor Epilepsy Center, Neurological Institute, Cleveland Clinic, Cleveland, Ohio, USA

[4]Department of Quantitative Health Sciences, Lerner Research Institute, Cleveland Clinic, Cleveland, Ohio, USA

Abstract

Focal cortical dysplasia (FCD) is associated with blood-brain barrier (BBB) dysfunction in patients with difficult-to-treat epilepsy. However, the underlying cellular and molecular factors in cortical dysplasia (CD) associated with progressive neurovascular challenges during the pro-epileptic phase, post-seizure and during epileptogenesis remain unclear. We studied the BBB function in a rat model of congenital (*in utero* radiation-induced, first hit) CD and longitudinally examined the cortical brain tissues at baseline and the progressive neurovascular alterations, glucose transporter-1 (GLUT1) expression and glucose metabolic activity at 2, 15, and 30 days following a second hit using pentylenetetrazole-induced seizure. Our study revealed through immunoblotting, immunohistochemistry and biochemical analysis that 1) altered vascular density and prolongation of BBB albumin leakages in CD rats continued through 30 days post-seizure, 2) CD brain tissues showed elevated matrix-metalloproteinase-9 levels at 2 days post-seizure and microglial overactivation through 30 days post-seizure, 3) BBB tight junction protein and GLUT1

*Corresponding Author: Chaitali Ghosh, PhD, Department of Biomedical Engineering (ND 20), Cleveland Clinic, 9500 Euclid Avenue, Cleveland, OH 44195 USA, Tel. 216/445-0559; Fax: 216/444-9198; GHOSHC@ccf.org.

Author Contributions:

C.G. designed the experiments and wrote the manuscript. R.M. performed the immunohistochemistry (DAB) staining, immunohistochemistry analyses, quantification and cell culture experiments. C.O., S.W., and M.N. cared for and treated the animals for the experiments and obtained the cortical brain tissues specimens used for analysis with the assistance of C.G. and I.N. In addition, S.W. performed initial histological and immunohistochemistry staining (fluorescent) and analysis. M.H. performed the western blot and biochemical assays. X.L. performed the statistical analysis of the data. All authors contributed to editing the manuscript.

Conflict of Interest: I.N. serves on the Speaker' bureau for Eisai, Inc, and as a member of ad hoc advisory board for Eisai, Inc and Liva Nova. None of the other authors has any potential conflict of interest to disclose.

Disclosure: We confirm that we have read the Journal's position on issues involved in ethical publication and affirm that this report is consistent with those guidelines.

Ethics Approval: All animal procedures were approved by the Animal Research Committee of Cleveland Clinic Foundation. All studies were performed in accordance with the approved guidelines by the Institutional Animal Care and Use Committee and the Institutional Biosafety Committee of Cleveland Clinic. All efforts were to minimize animal suffering.

levels were decreased and neuronal monocarboxylate transporter-2 (MCT2) and mammalian target of rapamycin (mTOR) levels were increased in the CD rat brain, 4) ATPase activity is elevated and a low glucose/high lactate imbalance exists in CD rats and 5) the mTOR pathway is activated and MCT2 levels are elevated in the presence of high lactate during glucose starvation *in vitro*. Together, this study suggests that BBB dysfunction, including decreased GLUT1 expression and metabolic disturbance, may contribute to epileptogenesis in this CD rat model through multiple mechanisms that could be translated to FCD therapy in medically refractory epilepsy.

Keywords

blood-brain barrier; epilepsy; tight junction proteins; glucose transporter-1; monocarboxylate transporter-2; mTOR

Introduction

The blood-brain barrier (BBB) is a critical physical and functional interface, protecting the brain from harmful substances in the bloodstream, while providing it with the required nutrients and a suitable microenvironment for normal neuronal function [1,2]. The role of BBB dysfunction in the pathophysiology of epilepsy has been well-recognized [3–6]. Evidence demonstrates that BBB breakdown may induce epileptic seizures, and this seizure-induced barrier disruption may cause subsequent epileptic episodes [5,6]. BBB dysfunction may be caused by several factors including inflammation, endothelial apoptosis, abnormal endothelial-glial interaction, loss of tight junction proteins and/or altered expression of multidrug transporters and enzymes [7,3,8]. BBB disruption facilitates seizure onset and long-lasting barrier breakdown, which can result in cognitive impairment [9,10,4,11]. Focal cortical dysplasia (FCD) is one of the most common epilepsy etiologies in children and adults, and the majority of patients do not respond to medications [12,13]. Although, the contribution of congenital dysplasia and seizures separately or in combination to neurovascular changes during disease progression has not been evaluated. The development of epilepsy could be a key transition period to investigate for improved therapeutic intervention in patients with cortical dysplasia (CD).

Previous studies have indicated that serum albumin leakage into the brain parenchyma may contribute to epileptogenesis [6] by lowering the threshold of spreading depolarization [14], inducing neuronal hyperexcitability and impairing neuronal function [15]. These neuronal functions could be worsened by glucose transporter-1 (GLUT1) dysfunction in the BBB and a glucose metabolic imbalance, which could be central regulators of altered physiology in epileptic pathologies [16,17]. Further, during epileptogenesis, these events leading to a compromised BBB could simultaneously dismantle the neurovascular bioenergetics and metabolic pathways. It has also been previously suggested that inhibition of mammalian target of rapamycin (mTOR) protects the functional integrity of the BBB in a preclinical mouse model of Alzheimer’s disease [18], while mutations involving mTOR pathway genes are commonly found in the focal brain region of patients with FCD [19–21]. Although, the cellular changes occurring at the BBB and to key metabolic pathways during epileptogenesis are still unclear in CD.

In this study, we aimed to examine the BBB structure in an animal model of congenital CD and evaluate the changes in the neurovasculature during epileptogenesis following an induced acute seizure. We determined (1) the gross histological neuronal and vascular structures and BBB dysfunction by FITC-albumin extravasation to the brain parenchyma, (2) the brain microglial activation pattern and extracellular matrix metalloproteinase-9 (MMP-9) levels, (3) the lasting effect of acute seizures on BBB integrity and tight junction protein (Claudin-5 and Claudin-1) levels, (4) cortical GLUT1, mTOR, monocarboxylate transporter-2 (MCT2) and glucose/lactate levels along with ATPase activity in the rat cortex and (5) mTOR pathway activation and MCT2 expression in the presence of lactate during glucose starvation *in vitro* to delineate the involvement of congenital cortical malformation and seizures in the cellular abnormalities relevant to the brain and vasculature function.

Materials and Methods

Animals

A total of 15 timed-pregnant Sprague-Dawley rats and their 84 male pups were used in this study (Charles River Laboratories, Wilmington, MA). Protocols for the care and use of the animals were approved by the Animal Research Committee of Cleveland Clinic Foundation. All studies were performed in accordance with the approved guidelines by the Institutional Animal Care and Use Committee and the Institutional Biosafety Committee of Cleveland Clinic. All rats included in the study were housed in individual cages, under 12-hour dark-light cycles, and had free access to food and water. Animals were housed in the Cleveland Clinic Biological Resources Unit accredited by the Association for Assessment and Accreditation of Laboratory Animal Care International.

In utero irradiation (XRT) for a model of cortical dysplasia (CD).—Ten timed-pregnant rats were irradiated with 145 cGy of cesium-137 on E17 for a model of multifocal cortical dysplasia as previously described [22,23]. An additional five timed-pregnant rats served as age-matched control animals. Date of birth usually occurred on E22, which was considered postnatal day 0 (PND0). All pups were grown to adulthood of PND45 prior to experimental procedures, which is when the non-CD and CD animals' overall body weights were quite comparable. A timeline of the experimental outline is depicted in Supplemental Fig. 1. Adult CD rats exhibit a decreased threshold to seizures, as the administration of a subconvulsive dose of pentylenetetrazole (PTZ) (40 mg/kg, i.p.) induces status epilepticus (SE) (second hit), as previously shown [22,23]. The same dose of PTZ was given to all rats that received the pro-convulsive agent. No seizures were detected in animals that did not receive PTZ. XRT+PTZ rats showed more severe seizures compared to PTZ rats, which had mild seizures at the given PTZ dose. Status epilepticus was followed by the emergence of interictal epileptic spikes in the majority of XRT+PTZ rats but not in normal rats with PTZ, as previously shown [22,24]. The patterns of seizure activity and severity in these rats was similar to that of our previously published studies [22,24]. More specifically, total seizure duration (in seconds) spent in Racine Stage 5 was found to be significantly more in XRT+PTZ compared to PTZ rats, as previously shown [22]. Rats that showed acute seizures after PTZ injection were used for further analysis in the respective groups. We longitudinally

studied the alterations in BBB and neuronal functions at various time points (2, 15 and 30 days) following PTZ-induced seizure in CD and normal rats.

Experimental usage of animals.—The 84 total animals used were split amongst the four experimental conditions – normal/control rat (NL), CD rat without seizure induction (XRT), normal rat with seizure induction (PTZ) and CD rat with seizure induction (XRT+PTZ) – for each of the three time points. Consequently, seven animals per condition, per time point were used for analysis. We dosed 42 total animals with PTZ for seizure/status epilepticus inductions. We used 21 animals for the PTZ group and 21 animals for the XRT+PTZ group. The perfused brains from these animals were either formalin-fixed (n=4/group for each time point) for histological or immunohistochemical analysis or snap frozen (n=3/group for each time point) for western blot, glucose/lactate measurement and ATPase activity assays.

FITC-albumin solution composition and treatment

A microangiographic technique based on the injection of fluorescent probes enables visualization of the entire brain microvasculature [25,26]. To this end, fluorescent albumin was used, since albumin does not extravasate abluminally if the BBB is intact [25,26]. In the present study, the fluorescent albumin solution was prepared by reconstituting 500 mg of bovine desiccate albumin-fluorescein isothiocyanate (FITC-albumin, MW 69 kDa; Sigma, St. Louis, MO) in 50 mL of phosphate buffered saline (0.1M PBS) lacking magnesium and calcium ions. FITC-albumin was directly infused in the left ventricle [25,26]. 10 mL of solution were injected at a rate of 1 mL/min under general anesthesia. The presence of vascular leakage in treated and control animals was evaluated by visual inspection and by fluorescent microscopy.

Histological and Immunohistochemical (IHC) Staining

The rat brain tissue was fixed immediately in 10% buffered formalin followed by 30% sucrose in PBS and sliced into 10 μm thick sections using a cryostat. IHC and histological staining were performed as previously described [8,27] on contiguous sections (n=5 each per specimen) obtained from rat brain tissues (experimental design outlined in Supplemental Fig. 1).

Histology.—Histopathology of the rat brain tissue was evaluated using cresyl violet (CV) staining on brain slices to identify the neuronal and general architectural organization pattern in the rat cortex regions.

Immunofluorescence.—Rat brain tissue slices were stained by IHC for various protein targets – NeuN, GFAP, Iba-1, and Claudin-5 (see Supplemental Table 1 for details) overnight at 4°C after blocking, followed by a two-hour incubation at room temperature with the corresponding fluorescent secondary antibody (Supplemental Table 1b). All sections were later mounted using Vectashield mounting medium with DAPI (H-1200, Vector Laboratories). Sections were then analyzed by fluorescence microscopy. Fluorescent images of the brain cortex were obtained using a Leica DM IL LED inverted microscope and a Leica DFC3000 G camera. The Leica LAS X program was used for image capture.

The acquired images were adjusted using ImageJ software (National Institute of Health, Bethesda, MD, USA).

Diaminobenzidine (DAB) Staining.—GLUT1, mTOR and MCT2 were evaluated using specific antibodies (Supplemental Table 1) in the brain sections obtained from XRT, PTZ, XRT+PTZ and normal (NL) rats at PND47, PND60 and PND75. The slices were permeabilized in 0.3% Tween in PBS, followed by blocking for endogenous peroxidase in 0.3% hydrogen peroxide in methanol and for non-specific binding in a solution of 5% goat serum and 0.4% Triton-X in PBS. The sections were incubated in wells with the primary antibody overnight with gentle shaking at 4°C, followed by a one hour incubation with the corresponding biotinylated secondary antibody (Supplemental Table 1). Sections were incubated for one hour with an avidin/biotin complex (Elite Vectastain ABC kit; PK-6100, Vector Labs, Burlingame, CA, USA). Thereafter, the antibody binding sites were visualized using DAB (without nickel solution; peroxidase substrate kit, SK-4100, Vector Labs), and mounted using Permount solution. Image acquisition of DAB-labeled sections was performed by brightfield microscopy, and the images obtained were adjusted with ImageJ software (National Institute of Health, Bethesda, MD, USA).

RECA-1 with CV staining.—The RECA-1 (Rat Endothelial Cell Antigen 1) DAB IHC and CV co-labelling for all groups (XRT, PTZ, and XRT+PTZ compared to normal) was performed to determine the vessel density changes in the cortical rat brain tissues at PND47, PND60 and PND75. As described above, the slices were processed using DAB staining with a primary anti-RECA-1 antibody (see Supplemental Table 1) overnight and, later, a biotinylated secondary antibody (Supplemental Table 1b) for one hour. The slides were subsequently processed for CV. This staining method allowed dual visualization of the cellular, especially neuronal, organization and the RECA-1-positive microvessels in the cortical brain slices, which were imaged by brightfield microscopy [28].

Image Analysis.—To quantify the IHC-positive staining, images of the brain cortex (n=5 images/rat/condition) of all groups were taken randomly (by a blinded-user) using Leica Application Suite 4.12 software (exposure 1.5 s, gain 1, gamma 0.93). Background was removed using the “rolling ball background subtraction” plugin for ImageJ with a radius of 50 pixels. The fluorescent images were split into channels using the “split channels” function, and the mean fluorescent intensity (fluorescent images) or threshold intensity (DAB images) and area of positive staining of each region of interest (ROI) were recorded. FITC-albumin extravasation was quantified by subtracting the fluorescent intensity of vessels in randomly chosen ROIs in the green channel using the Line Analyzer plugin in ImageJ from the total mean fluorescent intensity of the respective ROIs. Quantification of RECA-1 with CV histological stained slices in the microvessels was conducted by using a 5×5 grid (0.0625 mm^2) approach in ImageJ and counting the points of the grid where the vessels intersected the grid lines in four ROIs per image (modified from [29]). The process was repeated in different cortical areas of the RECA-1+ stained brain sections (n=3 images/rat/condition). The RECA-1+ vessel counts in XRT, PTZ and XRT+PTZ were compared to NL. Statistical analysis by one- or two-way ANOVA was subsequently performed based on the nature of the comparison being made.

Protein Isolation and Western Blot Analysis

Small portions of the snap-frozen rat brain tissues were homogenized in radio immunoprecipitation assay (RIPA) buffer (Sigma Aldrich, USA) with protease inhibitor (Sigma-Aldrich, USA). The tissue suspension was centrifuged at 14,000 rpm (Avanti-J25I, Beckman Coulter, USA); after, supernatant was collected, and the concentration of protein was measured by the Bradford method. Once all of the cortical tissue samples were collected from animals at each time point, protein isolation and western blots were performed simultaneously. MMP-9, Claudin-5, Claudin-1 and GLUT1 were separated by 10% and mTOR by 4–15% sodium dodecyl sulfate polyacrylamide gel electrophoresis (SDS-PAGE) and later transferred to polyvinylidene fluoride (PVDF) membranes (EMD Millipore Corp., Billerica, MA, USA) by semi-dry transfer (trans-Blot™ SD, Bio-Rad, USA). In brief, the membranes were probed overnight at 4°C with the respective primary antibody (listed in Supplemental Table 1a) followed by the appropriate secondary antibody (Supplemental Table 1b), as previously described [8]. For the target proteins, either the PVDF membranes were incubated in stripping buffer followed by blocking of the membranes or a fresh gel was repeated with the samples. Western blots were run in duplicates. In each case, the protein expression was normalized by β-actin (as loading control), and the densitometric quantification of the images was performed using ImageJ software (National Institute of Health, Bethesda, MD, USA). Throughout the study, animals were denoted in western blots by their assigned ID#: NL – PND47 (#1–3), PND60 (#13–15), PND75 (#25–27); XRT – PND47 (#4–6), PND60 (#16–18), PND75 (#28–30); PTZ – PND47 (#7–9), PND60 (#19–21), PND75 (#31–33); and XRT+PTZ – PND47 (#10–12), PND60 (#22–24), PND75 (#34–36).

Glucose and Lactate Measurement

Glucose and lactate were measured via a dual-channel immobilized oxidase enzyme analyzer (YSI 2700 SELECT; YSI Inc., Yellow Springs, OH) in rat brain tissue samples. The oxidase enzyme membrane integrity was made according to manufacturer recommendations. The glucose and lactate standards were used for calibration and validation of the protocol as previously described [30]. The detection ranges for D-glucose and L-lactate are 0–50 mmol/L and 0–29.98 mmol/L, respectively. D-glucose was calibrated to 13.89 mmol/L and L-lactate to 5.61 mmol/L. Glucose and lactate each has a coefficient of variation (CV) of 2% and a recovery of 97–100%. In brief, 50 mg of frozen brain tissue sample was homogenized in 300 μl of RIPA Buffer (Sigma, St. Louis, MO) with protease inhibitor cocktail (Sigma, St. Louis, MO). The tissue lysates were subsequently centrifuged for 30 min at 4°C, and the sample supernatants were analyzed consecutively. The glucose and lactate levels were measured in mmol/liter, and the data obtained for XRT, PTZ and XRT+PTZ groups at different time points were plotted relative to normal (NL) levels considered as 100%.

ATPase Assay

The ATPase activity from the brain tissue lysates of all groups (NL, XRT, PTZ, and XRT+PTZ) was measured by detecting the free inorganic phosphate (Pi) using a Pi-per Phosphate Assay kit (Molecular Probe, catalog # P22061). The assay measures an increase in fluorescence absorption of an Amplex Red reagent that is proportional to the amount

of Pi in the samples. Briefly, a standard curve was obtained by using different known concentrations of Pi. The standards and samples reacted with Amplex Red reagent for 60 min at 37°C in the dark. The Amplex Red reagent reaction product was detected fluorometrically using a fluorescence microplate reader (BioTek, Synergy HT, USA), with a setting for excitation at 530–560 nm and emission detection at 590 nm. The levels are represented as μmol of Pi per μg of protein in each specimen.

Cell Culture and Lactate Treatment

Human dopaminergic neuronal cells (DAN) derived from fetal brain tissues were purchased from Clonexpress (catalog number: DAN 020; Gaithersburg, MD, USA) and followed the company recommended culture media [31]. *Immunocytochemistry*. At approximately 75% confluency on coverslips, neuronal cells were fixed using 1% formalin and 4% sucrose in PBS (phosphate-buffered saline) for 45 min. Cells were then washed with 4% sucrose in PBS, blocked for 1 hour at room temperature and incubated overnight at 4°C using a mouse polyclonal anti-human microtubule associated protein 2 (MAP-2) primary antibody (1:200; Abcam Inc, Cambridge, MA, USA). FITC donkey anti-rabbit IgG secondary antibody (1:100 catalog number 711–095-152; Jackson Immunoresearch Inc., West Grove, PA, U.S.A.) was then used. Cells were mounted using Vectashield mounting medium with DAPI (H-1200, Vector Laboratories) and visualized with fluorescent microscopy as described above.

Human Embryonic Kidney (HEK) 293 cells were obtained from American Type Culture Collection (ATCC; catalog number: CRL-1573; Manassas, VA, U.S.A.) and grown in Dulbecco's modified eagle medium (DMEM, cat. no. 12430–054) with 10% fetal bovine serum (cat. no. 10100–147), both from Gibco, USA, 100 μg/ml penicillin and 100 μg/ml streptomycin.

Both cell types (DAN and HEK) in the treatment group were cultured separately in 100 mm petri dishes in complete medium containing 0 mM/low glucose with 20 mM lactate (sodium L-lactate, catalog number 71718 Sigma-Aldrich, USA) for 24 hours to mimic the low glucose/high lactate condition observed in the CD brain. Cells grown in normal DMEM or DAN media (both 0 mM lactate) were used as controls for HEK and neuronal cultures. After 24 hours, cells were lysed using RIPA lysis buffer with 1% protease inhibitor cocktail for western blot analysis. Cell lysates were separated through an 8% SDS gel and transferred onto PVDF membranes. The membranes were blocked and incubated with primary antibodies against mTOR, phospho-mTOR (Ser2448), phospho-S6K (Ser371), MCT2 or β-actin overnight at 4°C. The next day, the membranes were incubated with specific secondary antibodies for 1 hour at room temperature as described previously [27]. The antibody details are listed in Supplemental Table 1.

Statistical Analysis

All the statistical analyses in this study were performed on PC using 64-bit R-4.1.0 (R Foundation for Statistical Computing, Vienna, Austria. URL http://www.R-project.org/). Data were plotted using OriginPro 9.0 software (Origin Lab, Northampton, MA, USA).

IHC quantification analysis.—A two-way ANOVA model was used to analyze GLUT1, MCT2, and mTOR data, with IHC quantified values in four experimental groups (NL, XRT, PTZ, and XRT+PTZ) across three time points (PND47, PND60, and PND75). For each target, F test was performed to examine the overall difference across groups and time points and the interactions between groups and time points on the expression. When F test was significant overall, pairwise multiple comparison was further conducted to identify which specific means contributed to the significance. A Tukey *post hoc* test was used for pairwise comparison in order to control for the family-wise error rate resulting from multiple testing, and adjusted *p*-values were calculated to identify the significance of the difference in means between specific groups, time points and their interactions. We conducted one-way ANOVA and Tukey *post hoc* tests, given each time point, to identify the significant difference between specific treatment groups for RECA-1 and Iba-1.

Western blot quantification analysis and glucose, lactate and ATPase analysis.—A two-way ANOVA model was used to analyze MMP-9, Claudin-1, Claudin-5, GLUT1 and mTOR with western blot quantified values and glucose, lactate and ATPase assay values collected in the four groups across the three time points. We ran the same analytic procedure as described above in the IHC quantification analysis to identify any significant differences in mean expression between specific groups, time points and their interactions.

All data are shown as mean ± standard error of the mean (SEM). An adjusted *p*-value of <0.05 was considered statistically significant for all tests. All data collected in animals were from littermate controls and compared to experimental groups. No data were removed from the analyses, including statistical outliers.

Results

Alteration in vessel density, neuronal disorganization and FITC-albumin extravasation across the BBB in CD rats

Architectural disorganization in the cortex was demonstrated by gross histological, cresyl violet staining (Fig. 1a). Vessel density in the cortex was initially decreased in XRT rats compared to normal (Fig. 1a). Seizure induction in normal rats resulted in increased vessel density at 2 days post-PTZ and 15 days post-PTZ but not at 30 days post-PTZ. Although, a significant increase in vessel density was observed 2 days post-seizure induction in XRT+PTZ rats (**$p<0.01$), which was also present 30 days post-PTZ (***$p<0.001$) as compared to normal rats. Following acute seizure in dysplastic rats (XRT+PTZ), BBB damage was characterized by increased FITC-albumin extravasation to the brain parenchyma, starting at 2 days (Fig. 1b and Supplemental Fig. 2) and continuing through 15 and 30 days post-PTZ (Supplemental Fig. 2) compared to normal rats. FITC-albumin BBB leakages were mainly observed in XRT+PTZ and XRT rats around the cortical layers that displayed clustering of dysmorphic neurons (Fig. 1b). The mean level of FITC-albumin leakage was significantly increased in the XRT+PTZ cortex compared to that of the XRT (***$p<0.001$) and PTZ (***$p<0.001$) groups, determined by two-way ANOVA analysis (Supplemental Fig. 2).

Compromised BBB synchronizes with activated microglia and increased cortical MMP-9 levels

Our results show that microglial activation, identified by Iba-1 expression, was extensive in cortical brain regions of XRT and XRT+PTZ rats, particularly in the areas showing BBB disruption by FITC-albumin leakage in (Fig. 2a). High magnification images from the cortex of each group show a relatively increased number of Iba1-positive microglia in the XRT (***$p<0.001$), PTZ (*$p<0.05$) and XRT+PTZ (***$p<0.001$) rat brains compared to normal levels at PND47 (Fig. 2a). One-way ANOVA analysis of the PND47 results shows that the difference in Iba-1 activation between the XRT and XRT+PTZ groups was not significant ($p = 0.69$). Although, Iba-1 activation was significantly different between the PTZ and XRT+PTZ groups (***$p<0.001$) at PND47 or 2 days post-seizure. Iba-1 levels in the XRT+PTZ rats remained elevated at 15 days (***$p<0.001$) and 30 days (**$p<0.01$) post-seizure compared to the PTZ group (Fig. 2a). The glial (GFAP) activation or reactive gliosis of astrocytes (Supplemental Fig. 3) was not as robust as the microglial overactivation observed in XRT and XRT+PTZ brains (Fig. 2a). In conjunction with microglial activation, MMP-9 overexpression (Fig. 2b) was evident in the XRT+PTZ rat cortical tissues (**$p<0.01$) on 2 days post-PTZ (PND47) compared to normal brain tissues. By 15 days post-PTZ, MMP-9 levels decreased to baseline levels in all groups (Fig. 2b). All full western blots are shown in Supplemental Fig. 4.

Decreased tight junction proteins in areas with BBB leakage in the cortex of CD rats post-seizure induction

Tight junction proteins, Claudin-1 and Claudin-5, had variable expression patterns throughout the time points in the cortex of CD rats with and without seizure induction compared to normal (Fig. 3a). Two-way ANOVA shows that overall Claudin-1 expression significantly decreases over time (*$p = 0.041$), and there is a significant decrease in mean Claudin-1 levels in PND75 compared to PND47 (*$p = 0.038$). Claudin-1 expression was initially unchanged in XRT rats but then decreased by PND75 compared to normal (***$p<0.001$), while Claudin-1 expression in the PTZ group was decreased persistently from 2 days post-PTZ (**$p<0.01$) through 30 days post-PTZ (***$p<0.001$). However, Claudin-5 levels in the cortex showed a significant decrease in both XRT and PTZ rat brains at PND47, continuing through PND60 compared to normal. Interestingly, a significant and persistent downregulation of both Claudin-1 and Claudin-5 expression was observed in the brains of XRT+PTZ rats starting at 2 days through 30 days post-PTZ-induced seizures (Fig. 3a). Two-way ANOVA analysis shows a significant decrease in the mean XRT+PTZ cortical Claudin-5 level compared to mean Claudin-5 levels of the normal (***$p<0.001$) and PTZ (**$p<0.01$) groups. Although, the difference in mean Claudin-5 levels between the XRT and XRT+PTZ groups was not significant. However, there was a significant difference in the mean Claudin-1 levels between the normal (***$p<0.001$), XRT (***$p<0.001$) and PTZ (**$p<0.01$) compared to the XRT+PTZ group. At 30 days post-PTZ with a compromised BBB shown by FITC-albumin leakage, Claudin-5 expression remained low in the microvessels of XRT+PTZ rats compared to normal (Fig. 3b). The XRT and PTZ rat brains also showed a relative decrease in Claudin-5 immunostaining, suggesting a dysfunctional BBB compared to normal. In contrast, brain capillaries in the

normal cortex showed elevated Claudin-5 expression, indicative of a tighter barrier and negligible extravasation of FITC-albumin across the BBB (Fig. 3b).

Alterations of GLUT1 and glucose metabolism in the cortex of CD rats post-seizure

Compared to control brains, GLUT1 expression was significantly lower in the cortical tissue of XRT rats (**p<0.001) at PND47 and further decreased after seizure induction (XRT+PTZ, ***p<0.001). This significant and persistent decrease in GLUT1 expression in the XRT and XRT+PTZ rat cortices lasted through PND75, 30 days after PTZ-induced seizures (Fig. 4a). Overall, there is a significant decrease in GLUT1 expression in the XRT+PTZ group (***p<0.001) compared to the XRT group according to the pairwise comparison between the group means analyzed by two-way ANOVA. GLUT1 expression was mainly found in the microvessels of the normal cortex (Fig. 4b). The expression trend in the western blot is corroborated by the IHC staining of GLUT1 in these groups (Fig. 4b).

Subsequent measurements of the glucose and lactate levels in the same cortical tissues used for western blot confirm a significantly decreased glucose concentration in the XRT and XRT+PTZ cortices at PND47 compared to normal brains, which persisted through PND75 (Fig. 5a). Simultaneously increased lactate levels were found in the same rat groups, XRT and XRT+PTZ, at PND47 compared to normal brains (Fig. 5a). The absolute values of glucose and lactate (mmol/L) levels are also provided in Supplemental Fig. 5. All measured levels were within the linear range of the assay method, and the calculated glucose and lactate concentration in the sample ranged from 0.3 mmol/L to 1.31 mmol/L for glucose and from 0.6 mmol/L to 1.45 mmol/L for lactate. Greater energy consumption determined by elevated ATPase activity is also observed in the cortex of PTZ and XRT+PTZ at PND47 compared to normal (Fig. 5b). However, unlike in PTZ brain tissues, the ATPase activity remained elevated in XRT and XRT+PTZ rat cortices at PND60 and PND75 (Fig. 5b). Overall, there was a significant difference in the mean glucose level of the PTZ (***p<0.001) group, but not the XRT group (p = 0.09) compared to XRT+PTZ, according to two-way ANOVA analysis. This same trend is present in the lactate level analysis for the PTZ and XRT groups compared to XRT+PTZ (***p<0.001 and p = 0.99, respectively). Elevated MCT2 expression in the cortical neurons in the XRT and XRT+PTZ rat brains compared to normal lasted through PND75 (Fig. 5c). However, in the PTZ group, the MCT2 expression returned to control levels in the neurons by 30 days post-PTZ. There is a significant difference in the mean MCT2 expression levels between the PTZ and XRT+PTZ groups (***p<0.001), but not between XRT and XRT+PTZ (p = 0.078), determined by two-way ANOVA analysis. Also, overall MCT2 expression goes down with time, with a significant decrease in the mean MCT2 levels at PND75 compared to both PND47 (*p<0.05) and PND60 (***p<0.001).

Increased mTOR expression persists in CD rats after seizure induction, and mTOR activity is controlled by increased lactate levels *in vitro*

The mTOR levels in the cortex were found to be significantly increased in XRT and XRT+PTZ rats on PND47 compared to normal rats (Fig. 6a–b). mTOR staining was most pronounced in cortical neurons (Fig. 6a), where the mTOR levels remained consistently increased until PND75 (30 days post-PTZ) in XRT+PTZ rats (Fig. 6a–b). At 30 days

post-seizure, the PTZ rat cortical mTOR levels were also found to sporadically increase compared to normal (Fig. 6a–b). The combined mean mTOR expression level at all time points by pairwise group comparison of XRT+PTZ is significantly increased compared to that of XRT (***p<0.001) and PTZ (***p<0.001). Also, statistical analysis of the mTOR levels by IHC revealed that overall, mTOR expression increased over time, with significant increases in the mean levels in PND60 (***p<0.001) compared to PND47 and in PND75 (*p<0.05) compared to PND60. Lactate supplementation during glucose starvation upregulated lactate transporter, MCT2, and mTOR pathway proteins, mTOR, phospho-mTOR, phospho-ribosomal protein S6 kinase beta-1 (phospho-S6K) in both human normal dopaminergic neuronal cells (DAN, Fig. 6c) and HEK cells (a broadly used cell line that retains many properties of immature neurons) (Supplemental Fig. 6) [32].

Discussion

The dysplastic and pro-epileptic brain in the current study shows BBB dysfunction, with decreased levels of tight junction proteins and an endothelial glucose transporter, that is prolonged post-seizure induction in CD rats. The BBB alterations are accompanied by increased microglial activation, MMP-9 and mTOR protein expression in the CD brains. Hampered glucose transport to the brain through decreased GLUT1 in the BBB was elucidated by decreased brain glucose levels partnered with increased lactate levels in CD rats, while ATPase activity remained elevated. These changes were further accentuated and more persistent in the dysplastic brain during the period of epileptogenesis that was shown to occur following a “second hit” [22–24].

Loss of BBB integrity and altered microvessel density in rats with CD

BBB integrity is compromised in the *in utero* irradiation rodent model of CD during the pro-epileptic stage (XRT) and is further weakened during epileptogenesis following a “second hit” (XRT+PTZ). Previous studies have shown that BBB dysfunction is a hallmark of pathophysiological changes in epilepsy [3,33,4], and the degree of BBB dysfunction in humans often correlates with disease severity [34,8]. In fact, BBB disruption with microvascular permeability to serum macromolecules is one of the earliest events documented following status epilepticus [34–36,5]. The leaky barrier (identified by FITC-albumin extravasation) in the radiation-induced CD model, observed to be prolonged in our current study, could play a role in the previously reported decreased threshold to seizure induction [37,22,23]. We have also earlier shown that a “second hit” (e.g. provoked seizure or trauma) leads to the transformation of a pro-epileptic dysplasia into an epileptic pathology [22,24]. Recurrent seizures have also been noted to further compromise the BBB function and lead to the progression of epilepsy [38,4,5,8]. In the current study, we found that microvessel density increased following seizure induction in rats with and without CD. These findings may suggest that the increase in microvessel density that has been previously reported in patients with focal cortical dysplasia [39] could be triggered and prolonged by a “second hit,” resulting in epileptogenesis, rather than a consequence of the pro-epileptic substrate itself, where vessel density in this CD rat model without seizure induction is actually decreased [40].

Cortical microglial activation and MMP-9 level elevation with BBB leakages in CD rats following acute seizures

Ideally, the brain's internal milieu is immune-privileged and required for proper synaptic, neuronal and network activities. BBB breakdown due to seizure or underlying pathophysiological changes triggered by congenital stimulation results in pro-inflammatory activity and immune responses through activation of microglial cells and astrocytes [41]. Iba-1 is known to increase with microglial activation [42], where it may be involved in membrane ruffling and phagocytosis [43,44]. Overactivation of Iba-1 seen in rats after seizure induction was further exacerbated by the CD substrate, suggesting neuroinflammatory activity. We recently observed similar microglial changes in human FCD type II tissue resected from patients with medically intractable focal epilepsy (unpublished data). Extracellular matrix protein MMP-9 contributes to the remodeling of synapses, proteolytic action on the BBB and seizure induction [45] which we find elevated in the CD rats at 2 days after seizure. This finding suggests that the combination of the pro-epileptic substrate and a subsequent second-hit could compromise the extracellular matrix integrity, which is pivotal for the neurovascular interface.

Persistent decrease in tight junction proteins in CD rats following seizure induction

In our setting, decreased Claudin-1 and Claudin-5 levels and increased FITC-albumin extravasation to the brain parenchyma in CD rats lasted through 30 days post-seizure induction, indicating that the CD substrate exacerbates and prolongs the loss of tight junction proteins that has been observed following SE. Interestingly, based on the overall group analysis, it seems that the decrease in Claudin-1, but not Claudin-5, was worsened by seizure induction. Whereas, the decrease in Claudin-5 in CD rats with seizure induction can be attributed to the CD substrate, itself. The variable pattern of Claudin-1 and Claudin-5 expression that we have observed could be interesting to further investigate. Additionally, the compromised BBB integrity in this CD rat model is corroborated by previous studies from our group showing decreased Claudin-5, Claudin-1 and Occludin levels, with diffuse and discontinuous expression in blood vessels in brain regions with elevated IgG extravasation in human FCD [8] and in temporal lobe epilepsy by others [46], elucidating the important association between epilepsy and BBB integrity.

Impaired glucose metabolic activity in CD rats with alteration of neurovascular function

Our findings show a persistent decrease in GLUT1, an important BBB solute carrier protein, and subsequent glucose deprivation in CD rat brains prior to and during second hit-induced epileptogenesis. Additionally, cortical lactate levels were increased in these same animals. Cellular metabolism is a vital component of BBB function, balancing brain homeostasis and neuronal function. Glucose is the essential source of energy in the brain, and GLUT1 facilitates the transport of glucose across the plasma membranes of BBB endothelial cells [47]. Therefore, a dysfunctional glucose transporter mechanism at the BBB in CD rats could influence the glucose availability to the brain and, subsequently, metabolic activity. The lactate increase seen in the dysplastic cortex before and during epileptogenesis could represent an alternative energy source to compensate for the lack of glucose availability in the brain and meet the increased energy demands to sustain the elevated ATP consumption

observed in CD brains. Neurons have been found to utilize lactate, which is transported into these cells via MCT2, as an energy source [47]. Upregulated neuronal MCT2 expression observed in CD rats that continues post-SE may possibly lead to neuronal hyperexcitability during "stressful" conditions (e.g. during SE) [48], through the increased uptake of lactate into neurons, to offset the low-glucose environment.

In the current study, *in utero*-induced CD before and following an induced seizure was found to be associated with mTOR upregulation. The delayed increase in mTOR seen in PTZ rats could be due to the biphasic nature of mTOR activation that has previously been described in a kainic acid rat seizure model, where over the course of 5 weeks, mTOR activation rose and fell multiple times. Inhibition of mTOR by rapamycin before kainate in that same study was found to prevent epileptogenesis and seizure-induced elevation of mTOR activation [49]. mTOR signaling and GLUT1-facilitated glucose transport are critical elements for glucose regulation and metabolic activity, including rescue from cell starvation with lactate [50]. As we had confirmed *in vitro* with human dopaminergic neuronal cells and HEK as a "*proof of concept,"* the presence of exogenous lactate during glucose starvation activated the mTOR pathway and increased the expression of MCT2, so hypothesize that lactate levels in the CD brain could contribute to mTOR signaling overactivation in dysplastic brains. Both GLUT1 deficiency and mTOR overactivation and have been associated with genetically acquired seizures [51,52]. Interestingly, the mTOR pathway has previously been found to be inhibitory to glucose uptake and to alter GLUT1 localization in the liver of mice with mTOR hyperactivation due to tuberous sclerosis complex-1 knockout [53]. Overall, regulation of mTOR and GLUT1, and perhaps even an association between the two, at the neurovascular interface could be pivotal for brain metabolism and homeostasis in CD rats post-seizure, which could be further examined in the future.

Neurovascular alteration and GLUT1-associated metabolic disturbance in CD rat model with seizure induction

In conclusion, the two-hit CD rat model unveiled the critical relevance of a dysfunctional BBB, GLUT1-associated metabolic activity and neuronal connection found in the CD pathology (summarized in Fig. 7). The congenital CD substrate, which aggravates the pro-epileptic stage, coupled with seizure induction further sustains the elevated MMP-9 levels, microglial activation and subsequent BBB disruption with a decrease in the tight junction protein levels and increased albumin brain extravasation. The lower glucose and higher lactate levels in the brain possibly trigger the mTOR signaling pathway and a compensatory energy fueling mechanism aided by increased neuronal MCT2 in the CD brain. This metabolic disturbance at the neurovasculature could contribute to epileptogenesis and ictogenesis, which needs to be further investigated.

Supplementary Material

Refer to Web version on PubMed Central for supplementary material.

Funding:

This work is supported in part by the National Institute of Neurological Disorders and Stroke/National Institutes of Health grant R01NS095825.

Data Availability:

The data that support the findings of this study are available from the corresponding author upon reasonable request. Some data may not be made available because of privacy or ethical restrictions.

References

1. Neuwelt EA, Bauer B, Fahlke C, Fricker G, Iadecola C, Janigro D, Leybaert L, Molnar Z, O'Donnell ME, Povlishock JT, Saunders NR, Sharp F, Stanimirovic D, Watts RJ, Drewes LR (2011) Engaging neuroscience to advance translational research in brain barrier biology. Nat Rev Neurosci 12 (3):169–182. doi:10.1038/nrn2995 [PubMed: 21331083]
2. Zlokovic BV (2008) The blood-brain barrier in health and chronic neurodegenerative disorders. Neuron 57 (2):178–201. doi:10.1016/j.neuron.2008.01.003 [PubMed: 18215617]
3. Gorter JA, Aronica E, van Vliet EA (2019) The Roof is Leaking and a Storm is Raging: Repairing the Blood-Brain Barrier in the Fight Against Epilepsy. Epilepsy Curr 19 (3):177–181. doi:10.1177/1535759719844750 [PubMed: 31037960]
4. Seiffert E, Dreier JP, Ivens S, Bechmann I, Tomkins O, Heinemann U, Friedman A (2004) Lasting blood-brain barrier disruption induces epileptic focus in the rat somatosensory cortex. J Neurosci 24 (36):7829–7836. doi:10.1523/JNEUROSCI.1751-04.2004 [PubMed: 15356194]
5. van Vliet EA, da Costa Araujo S, Redeker S, van Schaik R, Aronica E, Gorter JA (2007) Blood-brain barrier leakage may lead to progression of temporal lobe epilepsy. Brain 130 (Pt 2):521–534. doi:10.1093/brain/awl318 [PubMed: 17124188]
6. Weissberg I, Reichert A, Heinemann U, Friedman A (2011) Blood-brain barrier dysfunction in epileptogenesis of the temporal lobe. Epilepsy Res Treat 2011:143908. doi:10.1155/2011/143908 [PubMed: 22937228]
7. Abbott NJ, Patabendige AA, Dolman DE, Yusof SR, Begley DJ (2010) Structure and function of the blood-brain barrier. Neurobiol Dis 37 (1):13–25. doi:10.1016/j.nbd.2009.07.030 [PubMed: 19664713]
8. Williams S, Hossain M, Ferguson L, Busch RM, Marchi N, Gonzalez-Martinez J, Perucca E, Najm IM, Ghosh C (2019) Neurovascular Drug Biotransformation Machinery in Focal Human Epilepsies: Brain CYP3A4 Correlates with Seizure Frequency and Antiepileptic Drug Therapy. Mol Neurobiol 56 (12):8392–8407. doi:10.1007/s12035-019-01673-y [PubMed: 31243719]
9. Raabe A, Schmitz AK, Pernhorst K, Grote A, von der Brelie C, Urbach H, Friedman A, Becker AJ, Elger CE, Niehusmann P (2012) Cliniconeuropathologic correlations show astroglial albumin storage as a common factor in epileptogenic vascular lesions. Epilepsia 53 (3):539–548. doi:10.1111/j.1528-1167.2012.03405.x [PubMed: 22372630]
10. Scott RC (2014) What are the effects of prolonged seizures in the brain? Epileptic Disord 16 Spec No 1:S6–11. doi:10.1684/epd.2014.0689 [PubMed: 25323416]
11. Tomkins O, Shelef I, Kaizerman I, Eliushin A, Afawi Z, Misk A, Gidon M, Cohen A, Zumsteg D, Friedman A (2008) Blood-brain barrier disruption in post-traumatic epilepsy. J Neurol Neurosurg Psychiatry 79 (7):774–777. doi:10.1136/jnnp.2007.126425 [PubMed: 17991703]
12. Lee SK, Kim DW (2013) Focal cortical dysplasia and epilepsy surgery. J Epilepsy Res 3 (2):43–47. doi:10.14581/jer.13009 [PubMed: 24649472]
13. Najm IM, Ying Z, Babb T, Mohamed A, Hadam J, LaPresto E, Wyllie E, Kotagal P, Bingaman W, Foldvary N, Morris H, Luders HO (2000) Epileptogenicity correlated with increased N-methyl-D-aspartate receptor subunit NR2A/B in human focal cortical dysplasia. Epilepsia 41 (8):971–976. doi:10.1111/j.1528-1157.2000.tb00281.x [PubMed: 10961623]

14. Lapilover EG, Lippmann K, Salar S, Maslarova A, Dreier JP, Heinemann U, Friedman A (2012) Peri-infarct blood-brain barrier dysfunction facilitates induction of spreading depolarization associated with epileptiform discharges. Neurobiol Dis 48 (3):495–506. doi:10.1016/j.nbd.2012.06.024 [PubMed: 22782081]
15. Ivens S, Gabriel S, Greenberg G, Friedman A, Shelef I (2010) Blood-brain barrier breakdown as a novel mechanism underlying cerebral hyperperfusion syndrome. J Neurol 257 (4):615–620. doi:10.1007/s00415-009-5384-z [PubMed: 20361293]
16. Leen WG, Taher M, Verbeek MM, Kamsteeg EJ, van de Warrenburg BP, Willemsen MA (2014) GLUT1 deficiency syndrome into adulthood: a follow-up study. J Neurol 261 (3):589–599. doi:10.1007/s00415-014-7240-z [PubMed: 24413642]
17. Stafstrom CE (2006) Epilepsy: a review of selected clinical syndromes and advances in basic science. J Cereb Blood Flow Metab 26 (8):983–1004. doi:10.1038/sj.jcbfm.9600265 [PubMed: 16437061]
18. Van Skike CE, Jahrling JB, Olson AB, Sayre NL, Hussong SA, Ungvari Z, Lechleiter JD, Galvan V (2018) Inhibition of mTOR protects the blood-brain barrier in models of Alzheimer's disease and vascular cognitive impairment. Am J Physiol Heart Circ Physiol 314 (4):H693–H703. doi:10.1152/ajpheart.00570.2017 [PubMed: 29351469]
19. Jansen LA, Mirzaa GM, Ishak GE, O'Roak BJ, Hiatt JB, Roden WH, Gunter SA, Christian SL, Collins S, Adams C, Riviere JB, St-Onge J, Ojemann JG, Shendure J, Hevner RF, Dobyns WB (2015) PI3K/AKT pathway mutations cause a spectrum of brain malformations from megalencephaly to focal cortical dysplasia. Brain 138 (Pt 6):1613–1628. doi:10.1093/brain/awv045 [PubMed: 25722288]
20. Lim JS, Kim WI, Kang HC, Kim SH, Park AH, Park EK, Cho YW, Kim S, Kim HM, Kim JA, Kim J, Rhee H, Kang SG, Kim HD, Kim D, Kim DS, Lee JH (2015) Brain somatic mutations in MTOR cause focal cortical dysplasia type II leading to intractable epilepsy. Nat Med 21 (4):395–400. doi:10.1038/nm.3824 [PubMed: 25799227]
21. Nakashima M, Saitsu H, Takei N, Tohyama J, Kato M, Kitaura H, Shiina M, Shirozu H, Masuda H, Watanabe K, Ohba C, Tsurusaki Y, Miyake N, Zheng Y, Sato T, Takebayashi H, Ogata K, Kameyama S, Kakita A, Matsumoto N (2015) Somatic Mutations in the MTOR gene cause focal cortical dysplasia type IIb. Ann Neurol 78 (3):375–386. doi:10.1002/ana.24444 [PubMed: 26018084]
22. Nemes AD, Ayasoufi K, Ying Z, Zhou QG, Suh H, Najm IM (2017) Growth Associated Protein 43 (GAP-43) as a Novel Target for the Diagnosis, Treatment and Prevention of Epileptogenesis. Sci Rep 7 (1):17702. doi:10.1038/s41598-017-17377-z [PubMed: 29255203]
23. Nemes AD, O'Dwyer R, Najm IM, Ying Z, Gonzalez-Martinez J, Alexopoulos AV (2017) Treatment with lacosamide impedes generalized seizures in a rodent model of cortical dysplasia. Epilepsia 58 (10):1755–1761. doi:10.1111/epi.13856 [PubMed: 28833036]
24. Oghlakian RO, Tilelli CQ, Hiremath GK, Alexopoulos AV, Najm IM (2009) Single injection of a low dose of pentylenetetrazole leads to epileptogenesis in an animal model of cortical dysplasia. Epilepsia 50 (4):801–810. doi:10.1111/j.1528-1167.2008.01815.x [PubMed: 19396951]
25. Cavaglia M, Dombrowski SM, Drazba J, Vasanji A, Bokesch PM, Janigro D (2001) Regional variation in brain capillary density and vascular response to ischemia. Brain Res 910 (1–2):81–93. doi:10.1016/s0006-8993(01)02637-3 [PubMed: 11489257]
26. Marchi N, Betto G, Fazio V, Fan Q, Ghosh C, Machado A, Janigro D (2009) Blood-brain barrier damage and brain penetration of antiepileptic drugs: role of serum proteins and brain edema. Epilepsia 50 (4):664–677. doi:10.1111/j.1528-1167.2008.01989.x [PubMed: 19175391]
27. Hossain M, Williams S, Ferguson L, Bingaman W, Ghosh A, Najm IM, Ghosh C (2020) Heat Shock Proteins Accelerate the Maturation of Brain Endothelial Cell Glucocorticoid Receptor in Focal Human Drug-Resistant Epilepsy. Mol Neurobiol. doi:10.1007/s12035-020-02043-9
28. Lauritzen F, Perez EL, Melillo ER, Roh JM, Zaveri HP, Lee TS, Wang Y, Bergersen LH, Eid T (2012) Altered expression of brain monocarboxylate transporter 1 in models of temporal lobe epilepsy. Neurobiol Dis 45 (1):165–176. doi:10.1016/j.nbd.2011.08.001 [PubMed: 21856423]
29. Hutter-Schmid B, Kniewallner KM, Humpel C (2015) Organotypic brain slice cultures as a model to study angiogenesis of brain vessels. Front Cell Dev Biol 3:52. doi:10.3389/fcell.2015.00052 [PubMed: 26389117]

30. Ghosh C, Hossain M, Mishra S, Khan S, Gonzalez-Martinez J, Marchi N, Janigro D, Bingaman W, Najm I (2018) Modulation of glucocorticoid receptor in human epileptic endothelial cells impacts drug biotransformation in an in vitro blood-brain barrier model. Epilepsia. doi:10.1111/epi.14567

31. Ghosh C, Hossain M, Spriggs A, Ghosh A, Grant GA, Marchi N, Perucca E, Janigro D (2015) Sertraline-induced potentiation of the CYP3A4-dependent neurotoxicity of carbamazepine: an in vitro study. Epilepsia 56 (3):439–449. doi:10.1111/epi.12923 [PubMed: 25656284]

32. Shaw G, Morse S, Ararat M, Graham FL (2002) Preferential transformation of human neuronal cells by human adenoviruses and the origin of HEK 293 cells. FASEB J 16 (8):869–871. doi:10.1096/fj.01-0995fje [PubMed: 11967234]

33. Loscher W, Potschka H, Sisodiya SM, Vezzani A (2020) Drug Resistance in Epilepsy: Clinical Impact, Potential Mechanisms, and New Innovative Treatment Options. Pharmacol Rev 72 (3):606–638. doi:10.1124/pr.120.019539 [PubMed: 32540959]

34. Friedman A (2011) Blood-brain barrier dysfunction, status epilepticus, seizures, and epilepsy: a puzzle of a chicken and egg? Epilepsia 52 Suppl 8:19–20. doi:10.1111/j.1528-1167.2011.03227.x [PubMed: 21967353]

35. Friedman A, Dingledine R (2011) Molecular cascades that mediate the influence of inflammation on epilepsy. Epilepsia 52 Suppl 3:33–39. doi:10.1111/j.1528-1167.2011.03034.x [PubMed: 21542844]

36. van Vliet EA, Aronica E, Gorter JA (2014) Role of blood-brain barrier in temporal lobe epilepsy and pharmacoresistance. Neuroscience 277:455–473. doi:10.1016/j.neuroscience.2014.07.030 [PubMed: 25080160]

37. Najm IM, Tilelli CQ, Oghlakian R (2007) Pathophysiological mechanisms of focal cortical dysplasia: a critical review of human tissue studies and animal models. Epilepsia 48 Suppl 2:21–32. doi:10.1111/j.1528-1167.2007.01064.x

38. Salar S, Maslarova A, Lippmann K, Nichtweiss J, Weissberg I, Sheintuch L, Kunz WS, Shorer Z, Friedman A, Heinemann U (2014) Blood-brain barrier dysfunction can contribute to pharmacoresistance of seizures. Epilepsia 55 (8):1255–1263. doi:10.1111/epi.12713 [PubMed: 24995798]

39. Wintermark P, Lechpammer M, Warfield SK, Kosaras B, Takeoka M, Poduri A, Madsen JR, Bergin AM, Whalen S, Jensen FE (2013) Perfusion Imaging of Focal Cortical Dysplasia Using Arterial Spin Labeling: Correlation With Histopathological Vascular Density. J Child Neurol 28 (11):1474–1482. doi:10.1177/0883073813488666 [PubMed: 23696629]

40. Deng Z, Huang H, Wu X, Wu M, He G, Guo J (2017) Distinct Expression of Various Angiogenesis Factors in Mice Brain After Whole-Brain Irradiation by X-ray. Neurochem Res 42 (2):625–633. doi:10.1007/s11064-016-2118-3 [PubMed: 27885577]

41. Vezzani A, Aronica E, Mazarati A, Pittman QJ (2013) Epilepsy and brain inflammation. Exp Neurol 244:11–21. doi:10.1016/j.expneurol.2011.09.033 [PubMed: 21985866]

42. Imai Y, Ibata I, Ito D, Ohsawa K, Kohsaka S (1996) A novel gene iba1 in the major histocompatibility complex class III region encoding an EF hand protein expressed in a monocytic lineage. Biochem Biophys Res Commun 224 (3):855–862. doi:10.1006/bbrc.1996.1112 [PubMed: 8713135]

43. Ito D, Imai Y, Ohsawa K, Nakajima K, Fukuuchi Y, Kohsaka S (1998) Microglia-specific localisation of a novel calcium binding protein, Iba1. Brain Res Mol Brain Res 57 (1):1–9. doi:10.1016/s0169-328x(98)00040-0 [PubMed: 9630473]

44. Ohsawa K, Imai Y, Kanazawa H, Sasaki Y, Kohsaka S (2000) Involvement of Iba1 in membrane ruffling and phagocytosis of macrophages/microglia. J Cell Sci 113 (Pt 17):3073–3084 [PubMed: 10934045]

45. Bronisz E, Kurkowska-Jastrzebska I (2016) Matrix Metalloproteinase 9 in Epilepsy: The Role of Neuroinflammation in Seizure Development. Mediators Inflamm 2016:7369020. doi:10.1155/2016/7369020 [PubMed: 28104930]

46. Liu JY, Thom M, Catarino CB, Martinian L, Figarella-Branger D, Bartolomei F, Koepp M, Sisodiya SM (2012) Neuropathology of the blood-brain barrier and pharmaco-resistance in human epilepsy. Brain 135 (Pt 10):3115–3133. doi:10.1093/brain/aws147 [PubMed: 22750659]

47. Jha MK, Morrison BM (2018) Glia-neuron energy metabolism in health and diseases: New insights into the role of nervous system metabolic transporters. Exp Neurol 309:23–31. doi:10.1016/j.expneurol.2018.07.009 [PubMed: 30044944]

48. Leroy C, Pierre K, Simpson IA, Pellerin L, Vannucci SJ, Nehlig A (2011) Temporal changes in mRNA expression of the brain nutrient transporters in the lithium-pilocarpine model of epilepsy in the immature and adult rat. Neurobiol Dis 43 (3):588–597. doi:10.1016/j.nbd.2011.05.007 [PubMed: 21624469]

49. Zeng LH, Rensing NR, Wong M (2009) The mammalian target of rapamycin signaling pathway mediates epileptogenesis in a model of temporal lobe epilepsy. J Neurosci 29 (21):6964–6972. doi:10.1523/JNEUROSCI.0066-09.2009 [PubMed: 19474323]

50. Huang C, Sheng S, Li R, Sun X, Liu J, Huang G (2015) Lactate promotes resistance to glucose starvation via upregulation of Bcl-2 mediated by mTOR activation. Oncol Rep 33 (2):875–884. doi:10.3892/or.2014.3655 [PubMed: 25484022]

51. Hegde M, Lowenstein DH (2014) The search for circulating epilepsy biomarkers. Biomark Med 8 (3):413–427. doi:10.2217/bmm.13.142 [PubMed: 24712433]

52. Marin-Valencia I, Good LB, Ma Q, Duarte J, Bottiglieri T, Sinton CM, Heilig CW, Pascual JM (2012) Glut1 deficiency (G1D): epilepsy and metabolic dysfunction in a mouse model of the most common human phenotype. Neurobiol Dis 48 (1):92–101. doi:10.1016/j.nbd.2012.04.011 [PubMed: 22683290]

53. Jiang X, Kenerson H, Aicher L, Miyaoka R, Eary J, Bissler J, Yeung RS (2008) The tuberous sclerosis complex regulates trafficking of glucose transporters and glucose uptake. Am J Pathol 172 (6):1748–1756. doi:10.2353/ajpath.2008.070958 [PubMed: 18511518]

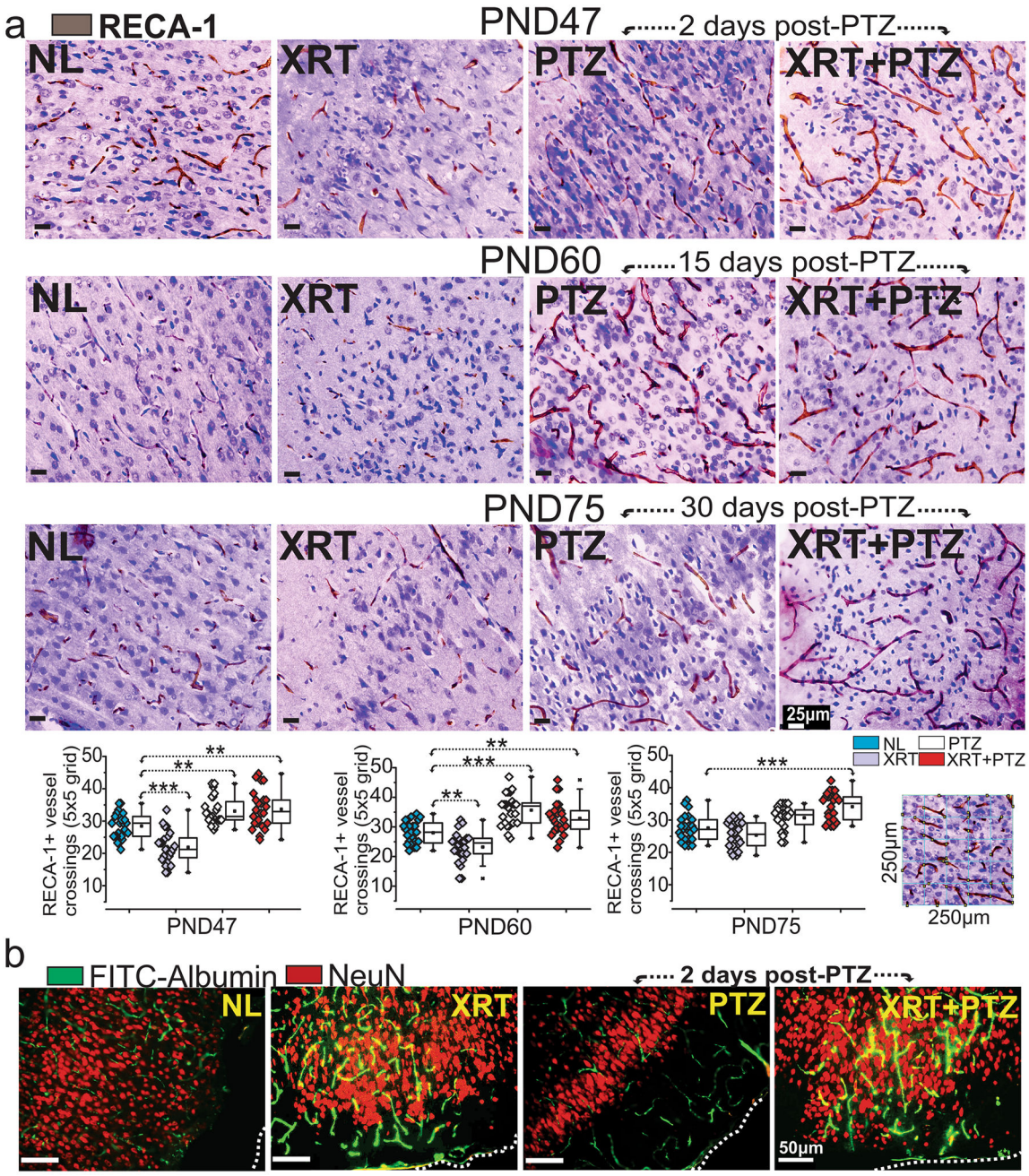

Fig. 1.

Cortical neuronal disorganization and BBB damage with altered vessel density in a rat model of CD. (**a**) Representative images of RECA-1 immunohistochemical staining and cresyl violet co-labelling of normal (NL), XRT, PTZ, and XRT+PTZ rat cortices and quantification of microvessel density. Microvessel density was increased in the cortex of PTZ rats but decreased in XRT compared to NL, both lasting until 15 days post-PTZ (PND60). XRT+PTZ rats showed an elevated microvessel density compared to NL that lasted through 30 days post-PTZ (PND75). Vessel density was quantified using a 5×5 region of interest grid (0.0625 mm^2) using ImageJ by counting the points of the grid where the

vessels contacted the grid lines [representative image of grid provided in (**a**)]. Statistical analysis by one-way ANOVA was performed on each time point independently with a Tukey *post-hoc* test, **p<0.01, ***p<0.001. Scale bar = 25 μm. (**b**) FITC-albumin (green) extravasation was evident throughout the cortex in XRT and XRT+PTZ rat brains compared to NL but was relatively less in PTZ rats. XRT and XRT+PTZ rats showed consistent neuronal disorganization in the cortex, with prominent FITC-albumin leakages compared to NL at PND47 (2 days post-PTZ). The neuronal marker NeuN (red) was used to label neuronal nuclei. Edge of cortex is outlined (white-dotted line) for reference. Scale bar = 50 μm

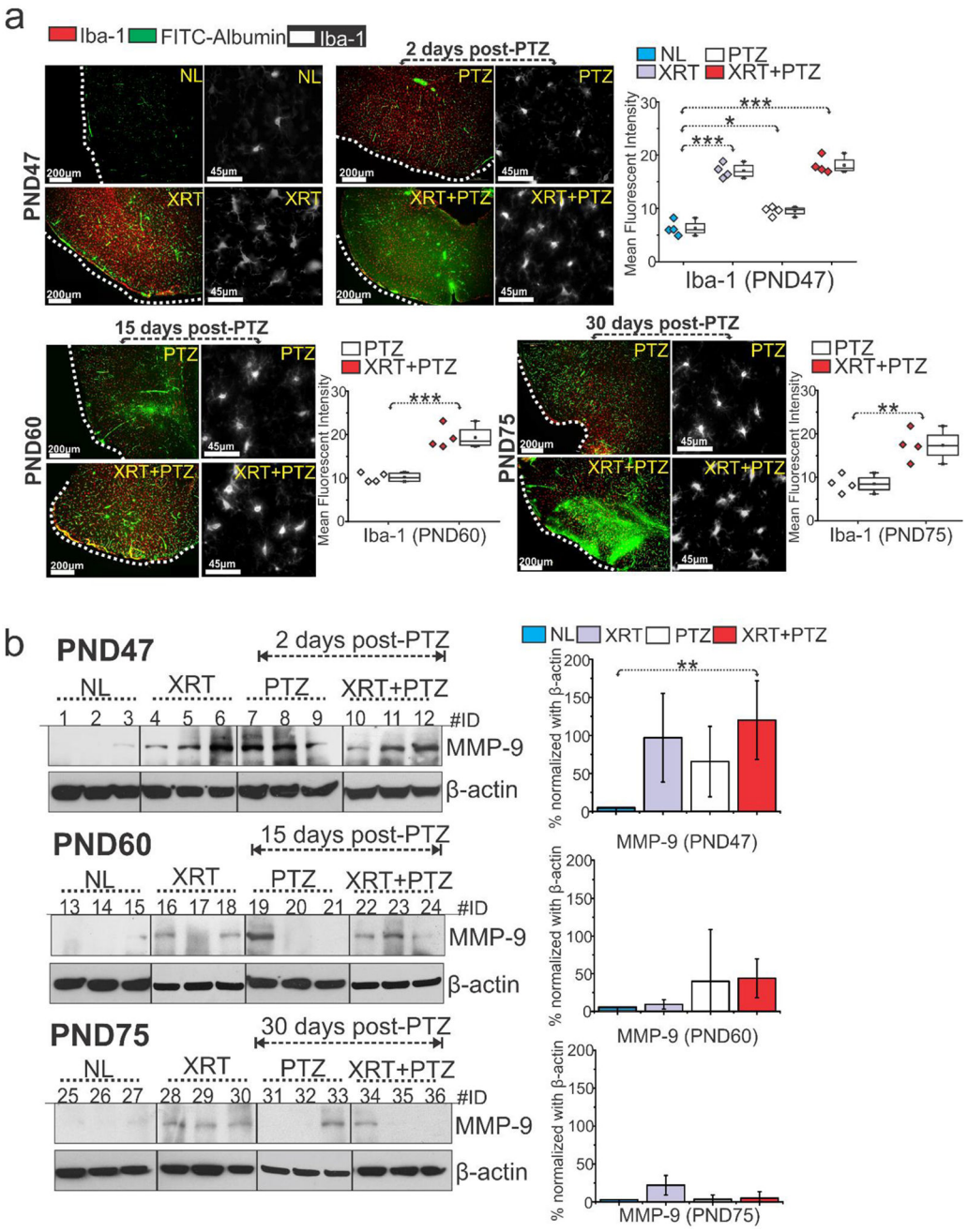

Fig. 2.

Microglial activation is elevated in the cortex with BBB leakages and overexpressed MMP-9 in CD rats with seizure induction. (**a**) Immunohistochemical staining of ionized calcium-binding adapter molecule 1 (Iba-1, red) and FITC-albumin (green) shows Iba-1 overactivity in the cortex of XRT, PTZ and XRT+PTZ compared to normal (NL) rat brains at 2 days post-PTZ (PND47). Grayscale high magnification (scale bar = 45 μm) images of cortical Iba-1 staining elucidate the level of microglial activation. The quantification of Iba-1 mean fluorescent intensity confirms increased activation of microglia in the XRT+PTZ cortex compared to the PTZ group at 15 and 30 days post-seizure. Iba-1 activation was

widespread in cortical areas with FITC-albumin extravasation in XRT and XRT+PTZ. Edge of cortex labeled with dotted line for reference. Results are expressed as mean ± SEM by one-way ANOVA, with each time point being analyzed independently, *p<0.05, **p<0.01, ***p<0.001. Scale bar = 200 μm for low magnification images. (**b**) Western blot shows a significant increase in MMP-9 (~92 kDa) levels in the XRT+PTZ rat cortex at PND47 (2 days post-PTZ) compared to NL levels. MMP-9 levels returned to NL by PND60 (15 days post-PTZ) in the XRT+PTZ group. The MMP-9 levels were negligible at PND75 in all groups. β-actin (~43 kDa) was used as a loading control and for normalization. The results are expressed as mean ± SEM by two-way ANOVA, **p<0.01

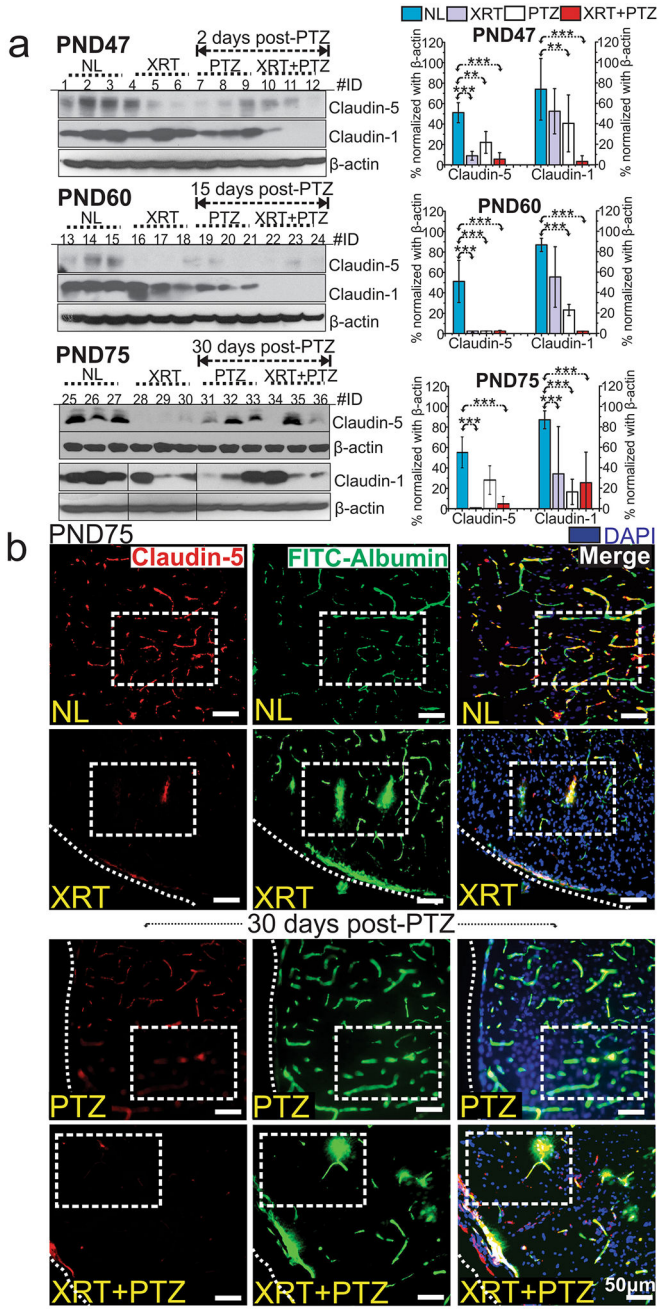

Fig. 3.

Decreased BBB tight junction protein levels in the cortex corroborate BBB disruption in seizure-induced rats with CD. (**a**) Western blot shows downregulated levels of Claudin-5 (~20 kDa) and Claudin-1 (~20 kDa) in XRT+PTZ rats at 2 days post-PTZ (PND47), which continued until 30 days post-PTZ (PND75) compared to normal (NL). Data are normalized with β-actin (~43 kDa), and values are plotted as mean ± SEM by two-way ANOVA for each target, **p<0.01, ***p<0.001. (**b**) Immunohistochemistry demonstrates decreased Claudin-5-positive staining in the microvessels, predominantly in areas with FITC-albumin extravasation (white-dotted box), in XRT and XRT+PTZ groups at PND75 (30 days post-

PTZ) compared to the normal (NL) rat cortex. Dotted line shows the edge of the cortex for reference. Scale bar = 50 μm

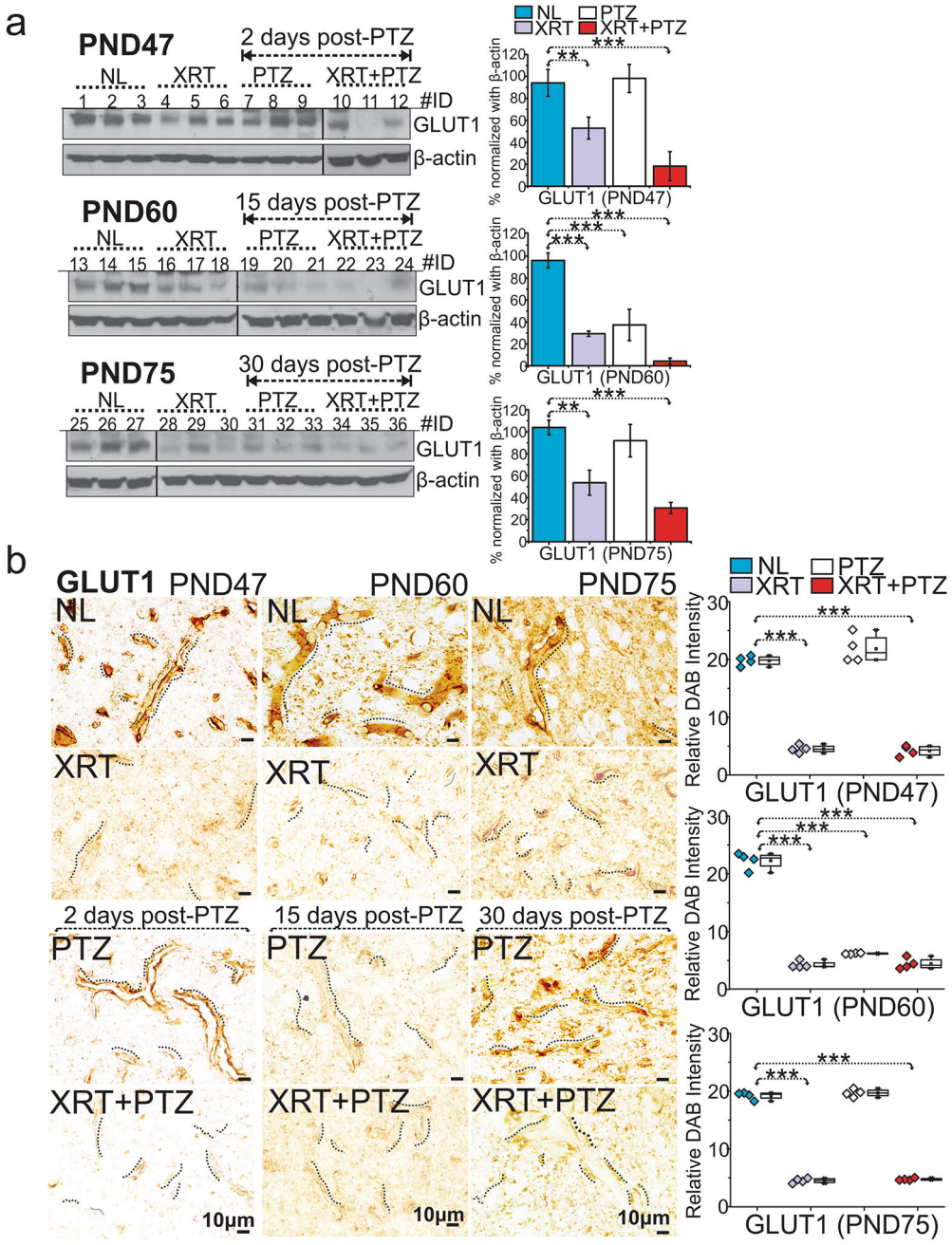

Fig. 4.

Decreased GLUT1 expression in CD rats with seizure induction. (**a**) Western blot shows significantly decreased GLUT1 (~56 kDa) levels in the cortex of XRT+PTZ and XRT vs. normal (NL) rats at PND47 (2 days post-PTZ) through PND75 (30 days post-PTZ). Data are normalized with β-actin (~43 kDa), and values are plotted as mean ± SEM by two-way ANOVA, **p<0.01, ***p<0.001. (**b**) GLUT1 localization is prominent across microvessels (indicated by dotted lines) in the NL rat cortex. GLUT1 levels were significantly decreased in XRT and XRT+PTZ rats at 2 days post-PTZ (PND47), 15 days post-PTZ (PND60) and 30 days post-PTZ (PND75) compared to NL rats. The PTZ rats showed a sporadic decrease

in GLUT1 at 15 days-post seizure (PND60). Quantification of relative DAB intensity is depicted as mean ± SEM by two-way ANOVA, ***p<0.001

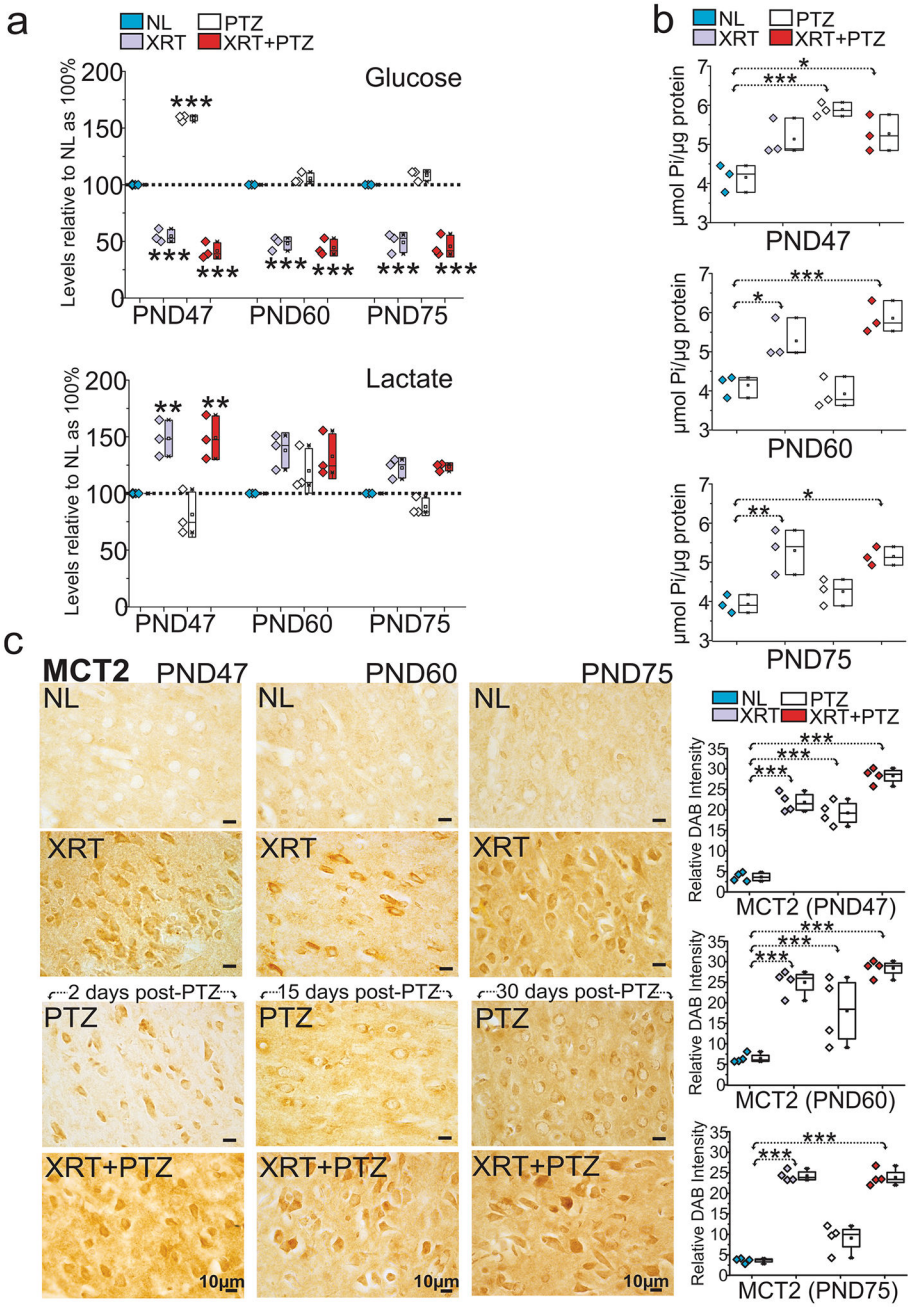

Fig. 5.

Glucose deprivation and lactate elevation in the cortex of CD rats with upregulated MCT2 expression and high ATPase activity. (**a**) Cortical glucose and lactate levels were measures in mmol/L in XRT, PTZ and XRT+PTZ rats and were plotted relative to normal (NL), considered as 100%. The glucose levels were significantly lower in XRT and XRT+PTZ compared to NL at PND47, PND60 and PND75. The PTZ group's glucose levels were significantly increased at PND47 but returned to NL by PND60. Simultaneously increased lactate levels were seen in XRT and XRT+PTZ rats at PND47 but returned back to normal by PND60. (**b**) Enhanced ATPase activity (µmol Pi/ per µg protein) in PTZ and XRT+PTZ

rats compared to NL is evident at PND47. The elevated ATPase activity was present only in XRT and XRT+PTZ at PND60 that persisted through PND75. (**c**) MCT2 expression, most prominent in cortical neurons, is significantly increased in XRT and XRT+PTZ compared to NL through PND75. However, MCT2 levels in PTZ rats are elevated through 15 days post-seizure but return to NL by 30 days post-seizure. All results (**a-c**) are expressed as mean ± SEM, and two-way ANOVA was used for statistical analysis of each target, *$p<0.05$, **$p<0.01$, ***$p<0.001$

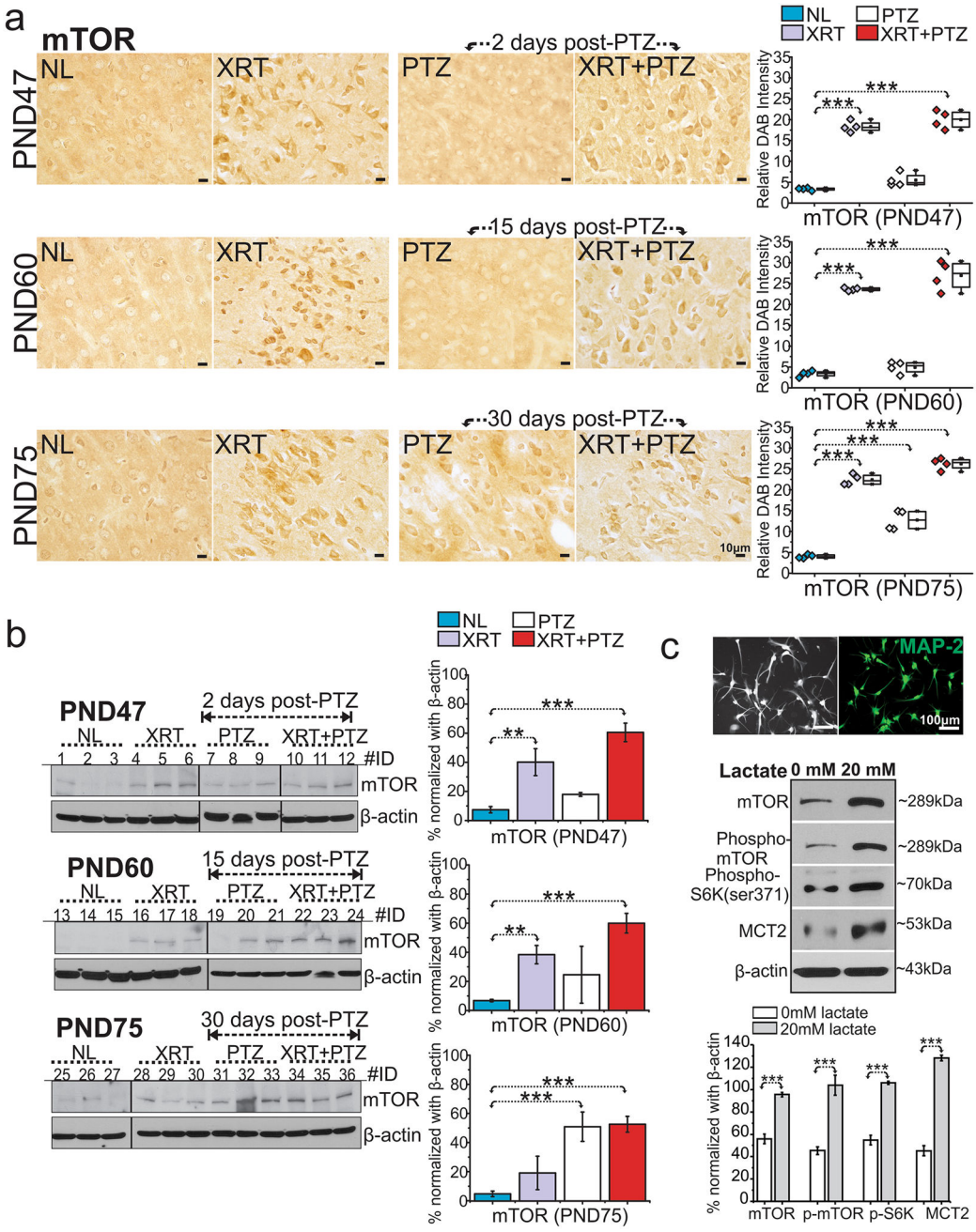

Fig. 6.

mTOR expression in the CD rat cortex remained elevated post-seizure induction, and lactate *in vitro* neuronal treatment increased mTOR signaling and MCT2 levels. (**a**) Immunohistochemistry showed mTOR expression most prominently across cortical neurons. mTOR expression in XRT and XRT+PTZ rats was elevated at PND47 (2 days post-seizure) and remained elevated through PND75 (30 days post-seizure) compared to normal (NL). By PND75, mTOR levels in the PTZ rat cortex were also increased. Scale bar = 10 μm. (**b**) Western blot shows increased mTOR (~289 kDa) levels in XRT+PTZ and XRT rats compared to NL at PND47 that remained elevated through PND75 in XRT+PTZ rats. mTOR

levels in PTZ rats showed a sporadic increase at PND75. **(c)** Immunocytochemistry was used to confirm neuronal cultures by fluorescent staining with MAP-2. Increased protein expression of mTOR, phospho-mTOR (Ser2448), phospho-S6K (Ser371) and MCT2 is found in human neuronal cells (DAN) after lactate treatment (20 mM) with low glucose (1 mM) vs. normal glucose media (0 mM lactate) control, examined by western blot. β-actin is used for normalization. The results are expressed as mean ± SEM by two-way ANOVA (a-b) and by two-sample t-test (c), **p<0.01, ***p<0.001

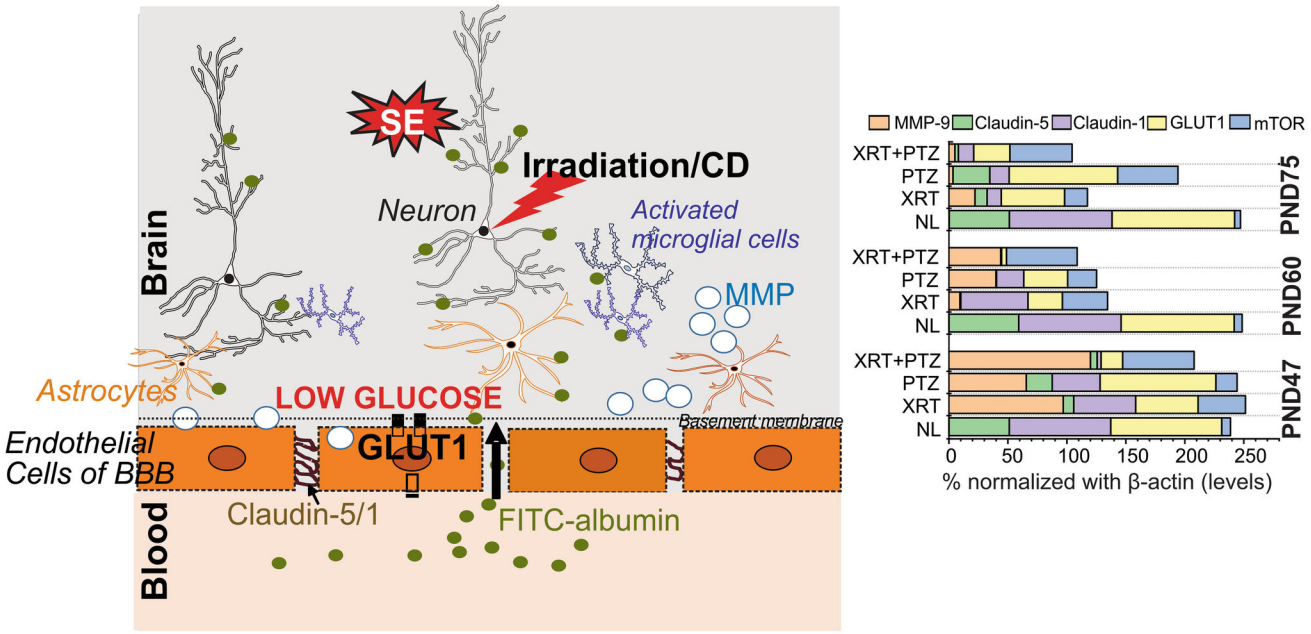

Fig. 7.

Schematic summary of neurovascular alterations in the CD rat model. Congenital irradiation-induced CD followed by status epilepticus (SE) triggered by a subconvulsive dose of PTZ was found to exaggerate (1) BBB leakage followed by FITC-albumin extravasation to the brain parenchyma showing neuronal disorganization, (2) an increase in MMP-9 levels and overactivation of microglial cells, (3) a decrease in tight junction protein (Claudin-1/−5) levels, compromising the BBB integrity, and (4) fluctuating brain metabolic activity (altered glucose-lactate levels) linking BBB to neuronal function. The mean levels of MMP-9, Claudin-1, Claudin-5, GLUT1 and mTOR in each of the groups at 2 days post-PTZ (PND47), 15 days post-PTZ (PND60) and 30 days post-PTZ (PND75) acquired from the western blot results are plotted in the top right to visualize the cumulative results of each target